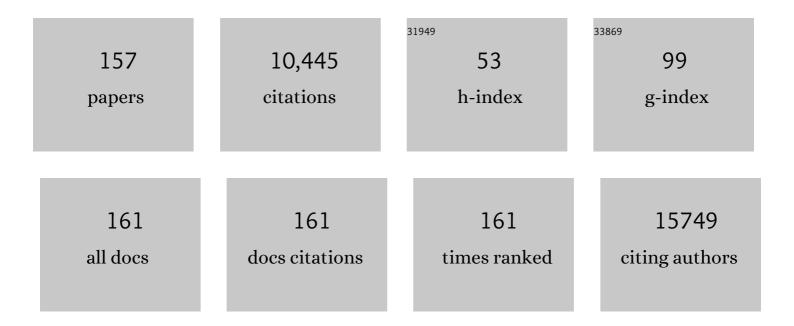
List of Publications by Year in descending order

Source: https://exaly.com/author-pdf/5023362/publications.pdf Version: 2024-02-01



#	Article	IF	CITATIONS
1	Selective Antisite Defect Formation in WS ₂ Monolayers via Reactive Growth on Dilute Wâ€Au Alloy Substrates. Advanced Materials, 2022, 34, e2106674.	11.1	14
2	Exploring the Spatial Control of Topotactic Phase Transitions Using Vertically Oriented Epitaxial Interfaces. Nano-Micro Letters, 2022, 14, 2.	14.4	3
3	Stabilized Synthesis of 2D Verbeekite: Monoclinic PdSe ₂ Crystals with High Mobility and In-Plane Optical and Electrical Anisotropy. ACS Nano, 2022, 16, 13900-13910.	7.3	14
4	Substoichiometric Tuning of the Electronic Properties of Titania. Thin Solid Films, 2021, 717, 138437.	0.8	6
5	Intrinsic Defects in MoS ₂ Grown by Pulsed Laser Deposition: From Monolayers to Bilayers. ACS Nano, 2021, 15, 2858-2868.	7.3	40
6	Strain-Induced Growth of Twisted Bilayers during the Coalescence of Monolayer MoS ₂ Crystals. ACS Nano, 2021, 15, 4504-4517.	7.3	19
7	Understanding Substrate-Guided Assembly in van der Waals Epitaxy by <i>in Situ</i> Laser Crystallization within a Transmission Electron Microscope. ACS Nano, 2021, 15, 8638-8652.	7.3	7
8	Investigating local oxidation processes in Fe thin films in a water vapor environment by in situ liquid cell TEM. Ultramicroscopy, 2020, 209, 112842.	0.8	11
9	Unusual electrical conductivity driven by localized stoichiometry modification at vertical epitaxial interfaces. Materials Horizons, 2020, 7, 3217-3225.	6.4	5
10	Permanently Magnetized Insulating Thinâ€Film Devices by Reduction. Physica Status Solidi - Rapid Research Letters, 2020, 14, 2000346.	1.2	0
11	Twoâ€Đimensional Palladium Diselenide with Strong Inâ€Plane Optical Anisotropy and High Mobility Grown by Chemical Vapor Deposition. Advanced Materials, 2020, 32, e1906238.	11.1	81
12	Low Energy Implantation into Transition-Metal Dichalcogenide Monolayers to Form Janus Structures. ACS Nano, 2020, 14, 3896-3906.	7.3	136
13	In situ laser reflectivity to monitor and control the nucleation and growth of atomically thin 2D materials*. 2D Materials, 2020, 7, 025048.	2.0	14
14	In Quest of a Ferromagnetic Insulator: Structure-Controlled Magnetism in Mg–Ti–O Thin Films. Journal of Physical Chemistry C, 2019, 123, 19970-19978.	1.5	8
15	Designing Morphotropic Phase Composition in BiFeO ₃ . Nano Letters, 2019, 19, 1033-1038.	4.5	24
16	lsotope-Engineering the Thermal Conductivity of Two-Dimensional MoS ₂ . ACS Nano, 2019, 13, 2481-2489.	7.3	42
17	Strain tolerance of two-dimensional crystal growth on curved surfaces. Science Advances, 2019, 5, eaav4028.	4.7	46
18	Defect-Mediated Phase Transformation in Anisotropic Two-Dimensional PdSe ₂ Crystals for Seamless Electrical Contacts. Journal of the American Chemical Society, 2019, 141, 8928-8936.	6.6	81

#	Article	IF	CITATIONS
19	Monolayer Ti ₃ C ₂ <i>T</i> _{<i>x</i>} as an Effective Co-catalyst for Enhanced Photocatalytic Hydrogen Production over TiO ₂ . ACS Applied Energy Materials, 2019, 2, 4640-4651.	2.5	177
20	Low-Temperature Charging Dynamics of the Ionic Liquid and Its Gating Effect on FeSe _{0.5} Te _{0.5} Superconducting Films. ACS Applied Materials & Interfaces, 2019, 11, 17979-17986.	4.0	10
21	2D/2D heterojunction of Ti ₃ C ₂ /g-C ₃ N ₄ nanosheets for enhanced photocatalytic hydrogen evolution. Nanoscale, 2019, 11, 8138-8149.	2.8	289
22	Roomâ€Temperature Insulating Ferromagnetic (Ni,Co) 1+2 x Ti 1â^' x O 3 Thin Films. Annalen Der Physik, 2019, 531, 1900299.	0.9	7
23	Realâ€Time Observation of Orderâ€Disorder Transformation of Organic Cations Induced Phase Transition and Anomalous Photoluminescence in Hybrid Perovskites. Advanced Materials, 2018, 30, e1705801.	11.1	60
24	The growth and assembly of organic molecules and inorganic 2D materials on graphene for van der Waals heterostructures. Carbon, 2018, 131, 246-257.	5.4	21
25	Influence of Nonstoichiometry on Proton Conductivity in Thin-Film Yttrium-Doped Barium Zirconate. ACS Applied Materials & Interfaces, 2018, 10, 4816-4823.	4.0	18
26	Vacuum-Assisted Low-Temperature Synthesis of Reduced Graphene Oxide Thin-Film Electrodes for High-Performance Transparent and Flexible All-Solid-State Supercapacitors. ACS Applied Materials & Interfaces, 2018, 10, 11008-11017.	4.0	57
27	Magnetic order multilayering in FeRh thin films by He-Ion irradiation. Materials Research Letters, 2018, 6, 106-112.	4.1	36
28	Self-Powered Fast Brazing of Ti-6Al-4V Using Ni/Al Reactive Multilayer Films. Applied Sciences (Switzerland), 2018, 8, 985.	1.3	10
29	Preparation of Thick Ni/Al Reactive Multilayer Films and Prospective Use for Self-Powered Brazing of Ti-6Al-4V. , 2018, , .		0
30	Speciation and Electronic Structure of La1â^'xSrxCoO3â^'δ During Oxygen Electrolysis. Topics in Catalysis, 2018, 61, 2161-2174.	1.3	25
31	In situ edge engineering in two-dimensional transition metal dichalcogenides. Nature Communications, 2018, 9, 2051.	5.8	100
32	The Influence of Local Distortions on Proton Mobility in Acceptor Doped Perovskites. Chemistry of Materials, 2018, 30, 4919-4925.	3.2	40
33	Layer-by-layer epitaxial thin films of the pyrochlore Tb ₂ Ti ₂ O ₇ . Nanotechnology, 2017, 28, 055708.	1.3	8
34	Black Anatase Formation by Annealing of Amorphous Nanoparticles and the Role of the Ti ₂ O ₃ Shell in Self-Organized Crystallization by Particle Attachment. ACS Applied Materials & Interfaces, 2017, 9, 22018-22025.	4.0	15
35	Vacancy filled nickelâ€cobaltâ€titanate thin films. Physica Status Solidi (B): Basic Research, 2017, 254, 1600799.	0.7	5
36	Edge-Controlled Growth and Etching of Two-Dimensional GaSe Monolayers. Journal of the American Chemical Society, 2017, 139, 482-491.	6.6	65

#	Article	IF	CITATIONS
37	Nanostructured carbon electrocatalyst supports for intermediate-temperature fuel cells: Single-walled versus multi-walled structures. Journal of Power Sources, 2017, 337, 145-151.	4.0	12
38	PdSe ₂ : Pentagonal Two-Dimensional Layers with High Air Stability for Electronics. Journal of the American Chemical Society, 2017, 139, 14090-14097.	6.6	509
39	The Role of Ru Redox in pH-Dependent Oxygen Evolution on Rutile Ruthenium Dioxide Surfaces. CheM, 2017, 2, 668-675.	5.8	151
40	UV-activated ZnO films on a flexible substrate for room temperature O2 and H2O sensing. Scientific Reports, 2017, 7, 6053.	1.6	61
41	Bottom up synthesis of boron-doped graphene for stable intermediate temperature fuel cell electrodes. Carbon, 2017, 123, 605-615.	5.4	23
42	Nonequilibrium Synthesis of TiO ₂ Nanoparticle "Building Blocks―for Crystal Growth by Sequential Attachment in Pulsed Laser Deposition. Nano Letters, 2017, 17, 4624-4633.	4.5	33
43	Suppression of Defects and Deep Levels Using Isoelectronic Tungsten Substitution in Monolayer MoSe ₂ . Advanced Functional Materials, 2017, 27, 1603850.	7.8	84
44	Stabilizing Ir(001) Epitaxy on Yttria-Stabilized Zirconia Using a Thin Ir Seed Layer Grown by Pulsed Laser Deposition. Crystal Growth and Design, 2017, 17, 89-94.	1.4	3
45	Growth control of oxygen stoichiometry in homoepitaxial SrTiO3 films by pulsed laser epitaxy in high vacuum. Scientific Reports, 2016, 6, 19941.	1.6	75
46	Low thermal budget, photonic-cured compact TiO ₂ layers for high-efficiency perovskite solar cells. Journal of Materials Chemistry A, 2016, 4, 9685-9690.	5.2	46
47	Persistent photoconductivity in two-dimensional Mo _{1â^'<i>x</i>} W _{<i>x</i>} Se ₂ –MoSe ₂ van der Waals heterojunctions. Journal of Materials Research, 2016, 31, 923-930.	1.2	20
48	Ultrafast Dynamics of Metal Plasmons Induced by 2D Semiconductor Excitons in Hybrid Nanostructure Arrays. ACS Photonics, 2016, 3, 2389-2395.	3.2	42
49	Isoelectronic Tungsten Doping in Monolayer MoSe ₂ for Carrier Type Modulation. Advanced Materials, 2016, 28, 8240-8247.	11.1	85
50	Tailoring Vacancies Far Beyond Intrinsic Levels Changes the Carrier Type and Optical Response in Monolayer MoSe _{2â^'<i>x</i>} Crystals. Nano Letters, 2016, 16, 5213-5220.	4.5	121
51	Two-dimensional GaSe/MoSe ₂ misfit bilayer heterojunctions by van der Waals epitaxy. Science Advances, 2016, 2, e1501882.	4.7	239
52	Ultrafast Charge Transfer and Hybrid Exciton Formation in 2D/0D Heterostructures. Journal of the American Chemical Society, 2016, 138, 14713-14719.	6.6	102
53	Observation of Nanoscale Morphological and Structural Degradation in Perovskite Solar Cells by in Situ TEM. ACS Applied Materials & amp; Interfaces, 2016, 8, 32333-32340.	4.0	54
54	Interlayer Coupling in Twisted WSe ₂ /WS ₂ Bilayer Heterostructures Revealed by Optical Spectroscopy. ACS Nano, 2016, 10, 6612-6622.	7.3	249

#	Article	IF	CITATIONS
55	Low temperature synthesis of hierarchical TiO ₂ nanostructures for high performance perovskite solar cells by pulsed laser deposition. Physical Chemistry Chemical Physics, 2016, 18, 27067-27072.	1.3	29
56	Carbon Nanotubes Grown on Metal Microelectrodes for the Detection of Dopamine. Analytical Chemistry, 2016, 88, 645-652.	3.2	113
57	Deciphering Halogen Competition in Organometallic Halide Perovskite Growth. Journal of the American Chemical Society, 2016, 138, 5028-5035.	6.6	92
58	Thickness-dependent charge transport in few-layer MoS ₂ field-effect transistors. Nanotechnology, 2016, 27, 165203.	1.3	124
59	Ultrathin nanosheets of CrSiTe ₃ : a semiconducting two-dimensional ferromagnetic material. Journal of Materials Chemistry C, 2016, 4, 315-322.	2.7	235
60	Observation of two distinct negative trions in tungsten disulfide monolayers. Physical Review B, 2015, 92, .	1.1	44
61	Controllable Growth of Perovskite Films by Roomâ€Temperature Air Exposure for Efficient Planar Heterojunction Photovoltaic Cells. Angewandte Chemie - International Edition, 2015, 54, 14862-14865.	7.2	41
62	Revealing the Preferred Interlayer Orientations and Stackings of Twoâ€Dimensional Bilayer Gallium Selenide Crystals. Angewandte Chemie, 2015, 127, 2750-2755.	1.6	5
63	High-Performance Flexible Perovskite Solar Cells by Using a Combination of Ultrasonic Spray-Coating and Low Thermal Budget Photonic Curing. ACS Photonics, 2015, 2, 680-686.	3.2	268
64	Revealing the Preferred Interlayer Orientations and Stackings of Twoâ€Dimensional Bilayer Gallium Selenide Crystals. Angewandte Chemie - International Edition, 2015, 54, 2712-2717.	7.2	45
65	Van der Waals Epitaxial Growth of Two-Dimensional Single-Crystalline GaSe Domains on Graphene. ACS Nano, 2015, 9, 8078-8088.	7.3	103
66	Patterned arrays of lateral heterojunctions within monolayer two-dimensional semiconductors. Nature Communications, 2015, 6, 7749.	5.8	213
67	Perovskite Solar Cells with Near 100% Internal Quantum Efficiency Based on Large Single Crystalline Grains and Vertical Bulk Heterojunctions. Journal of the American Chemical Society, 2015, 137, 9210-9213.	6.6	246
68	Structure and Formation Mechanism of Black TiO ₂ Nanoparticles. ACS Nano, 2015, 9, 10482-10488.	7.3	170
69	Anorthite sputtering by H ⁺ and Ar ^{<i>q</i>+} (<i>q</i> = 1–9) at solar wind velocities. Journal of Geophysical Research: Space Physics, 2014, 119, 8006-8016.	0.8	14
70	Exploring growth kinetics of carbon nanotube arrays by in situ optical diagnostics and modeling. Proceedings of SPIE, 2014, , .	0.8	0
71	Catalytic nanoparticles for carbon nanotube growth synthesized by through thin film femtosecond laser ablation. Proceedings of SPIE, 2014, , .	0.8	1
72	Slowing of femtosecond laser-generated nanoparticles in a background gas. Applied Physics Letters, 2014, 105, 213108.	1.5	6

#	Article	IF	CITATIONS
73	Cooperative Island Growth of Large-Area Single-Crystal Graphene on Copper Using Chemical Vapor Deposition. ACS Nano, 2014, 8, 5657-5669.	7.3	91
74	The isotopic effects of deuteration on optoelectronic properties of conducting polymers. Nature Communications, 2014, 5, 3180.	5.8	103
75	Pulsed Laser Deposition of Photoresponsive Twoâ€Dimensional GaSe Nanosheet Networks. Advanced Functional Materials, 2014, 24, 6365-6371.	7.8	108
76	Digital Transfer Growth of Patterned 2D Metal Chalcogenides by Confined Nanoparticle Evaporation. ACS Nano, 2014, 8, 11567-11575.	7.3	47
77	Nanoparticle generation and transport resulting from femtosecond laser ablation of ultrathin metal films: Time-resolved measurements and molecular dynamics simulations. Applied Physics Letters, 2014, 104, .	1.5	42
78	Revealing the surface and bulk regimes of isothermal graphene nucleation and growth on Ni with in situ kinetic measurements and modeling. Carbon, 2014, 79, 256-264.	5.4	16
79	Controlled Vapor Phase Growth of Single Crystalline, Two-Dimensional GaSe Crystals with High Photoresponse. Scientific Reports, 2014, 4, 5497.	1.6	222
80	Real-time optical diagnostics of graphene growth induced by pulsed chemical vapor deposition. Nanoscale, 2013, 5, 6507.	2.8	22
81	Nature of the band gap and origin of the electro-/photo-activity of Co3O4. Journal of Materials Chemistry C, 2013, 1, 4628.	2.7	176
82	Fluorination of "brick and mortar―soft-templated graphitic ordered mesoporous carbons for high power lithium-ion battery. Journal of Materials Chemistry A, 2013, 1, 9414.	5.2	23
83	Excimer laser reduction and patterning of graphite oxide. Carbon, 2013, 53, 81-89.	5.4	107
84	A water-soluble polythiophene for organic field-effect transistors. Polymer Chemistry, 2013, 4, 5270.	1.9	78
85	High-temperature transformation of Fe-decorated single-wall carbon nanohorns to nanooysters: a combined experimental and theoretical study. Nanoscale, 2013, 5, 1849-1857.	2.8	10
86	Uniform, Homogenous Coatings of Carbon Nanohorns on Arbitrary Substrates from Common Solvents. ACS Applied Materials & Interfaces, 2013, 5, 13153-13160.	4.0	23
87	Spatial and temporal measurements of temperature and cell viability in response to nanoparticle-mediated photothermal therapy. Nanomedicine, 2012, 7, 1729-1742.	1.7	14
88	Atomic Layer Engineering of Perovskite Oxides for Chemically Sharp Heterointerfaces. Advanced Materials, 2012, 24, 6423-6428.	11.1	49
89	Nanoengineering: Atomic Layer Engineering of Perovskite Oxides for Chemically Sharp Heterointerfaces (Adv. Mater. 48/2012). Advanced Materials, 2012, 24, 6422-6422.	11.1	0
90	Metal-assisted hydrogen storage on Pt-decorated single-walled carbon nanohorns. Carbon, 2012, 50, 4953-4964.	5.4	69

#	Article	IF	CITATIONS
91	Nonequilibrium laser synthesis and real-time diagnostics of carbon nanomaterial growth. , 2012, , .		0
92	Incremental Growth of Short SWNT Arrays by Pulsed Chemical Vapor Deposition. Small, 2012, 8, 1534-1542.	5.2	9
93	An integrated portable Raman sensor with nanofabricated gold bowtie array substrates for energetics detection. Analyst, The, 2011, 136, 1697.	1.7	25
94	Flux-Dependent Growth Kinetics and Diameter Selectivity in Single-Wall Carbon Nanotube Arrays. ACS Nano, 2011, 5, 8311-8321.	7.3	33
95	The use of low-energy SIMS (LE-SIMS) for nanoscale fuel cell material development. Surface and Interface Analysis, 2011, 43, 635-638.	0.8	3
96	Antioxidant Deactivation on Graphenic Nanocarbon Surfaces. Small, 2011, 7, 2775-2785.	5.2	133
97	Single walled carbon nanohorns as photothermal cancer agents. Lasers in Surgery and Medicine, 2011, 43, 43-51.	1.1	67
98	PSâ€ <i>b</i> â€₽3HT Copolymers as P3HT/PCBM Interfacial Compatibilizers for High Efficiency Photovoltaics. Advanced Materials, 2011, 23, 5529-5535.	11.1	110
99	Quantitative determination of energy enhanced interlayer transport in pulsed laser deposition of SrTiO3. Physical Review B, 2011, 84, .	1.1	15
100	Anomalous Oxidation States in Multilayers for Fuel Cell Applications. Advanced Functional Materials, 2010, 20, 2664-2674.	7.8	20
101	Functionally graded hydroxyapatite coatings doped with antibacterial components. Acta Biomaterialia, 2010, 6, 2264-2273.	4.1	143
102	Narrow and intense resonances in the low-frequency region of surface-enhanced Raman spectra of single-wall carbon nanotubes. Physical Review B, 2010, 82, .	1.1	8
103	Pulsed Growth of Vertically Aligned Nanotube Arrays with Variable Density. ACS Nano, 2010, 4, 7573-7581.	7.3	41
104	In Vitro and in Vivo Studies of Single-Walled Carbon Nanohorns with Encapsulated Metallofullerenes and Exohedrally Functionalized Quantum Dots. Nano Letters, 2010, 10, 2843-2848.	4.5	56
105	A Facile High-speed Vibration Milling Method to Water-disperse Single-walled Carbon Nanohorns. Chemistry of Materials, 2010, 22, 347-351.	3.2	22
106	Model for Self-Assembly of Carbon Nanotubes from Acetylene Based on Real-Time Studies of Vertically Aligned Growth Kinetics. Journal of Physical Chemistry C, 2009, 113, 15484-15491.	1.5	59
107	Cumulative and continuous laser vaporization synthesis of single wall carbon nanotubes and nanohorns. Applied Physics A: Materials Science and Processing, 2008, 93, 849-855.	1.1	34
108	Interfaces in perovskite heterostructures. Applied Physics A: Materials Science and Processing, 2008, 93, 807-811.	1.1	12

#	Article	IF	CITATIONS
109	Altering the catalytic activity of thin metal catalyst films forÂcontrolled growth of chemical vapor deposited vertically aligned carbon nanotube arrays. Applied Physics A: Materials Science and Processing, 2008, 93, 1005-1009.	1.1	8
110	Pulsed laser CVD investigations of single-wall carbon nanotube growth dynamics. Applied Physics A: Materials Science and Processing, 2008, 93, 987-993.	1.1	25
111	Real-time imaging of vertically aligned carbon nanotube array growth kinetics. Nanotechnology, 2008, 19, 055605.	1.3	61
112	In situ timeâ€resolved measurements of carbon nanotube and nanohorn growth. Physica Status Solidi (B): Basic Research, 2007, 244, 3944-3949.	0.7	18
113	Normal-incidence generalized ellipsometry using the two-modulator generalized ellipsometry microscope. Applied Optics, 2006, 45, 5479.	2.1	25
114	Generalized ellipsometry in unusual configurations. Applied Surface Science, 2006, 253, 47-51.	3.1	2
115	Nonequilibrium Interlayer Transport in Pulsed Laser Deposition. Physical Review Letters, 2006, 96, 226104.	2.9	46
116	R&D of RABiTS-based coated conductors: Conversion of ex situ YBCO superconductor using a novel pulsed electron-beam deposited precursor. Physica C: Superconductivity and Its Applications, 2005, 426-431, 878-886.	0.6	9
117	Nanoscale effects on the ionic conductivity in highly textured YSZ thin films. Solid State Ionics, 2005, 176, 1319-1326.	1.3	330
118	Strong polarization enhancement in asymmetric three-component ferroelectric superlattices. Nature, 2005, 433, 395-399.	13.7	627
119	Germanium-Catalyzed Growth of Zinc Oxide Nanowires: A Semiconductor Catalyst for Nanowire Synthesis. Angewandte Chemie - International Edition, 2005, 44, 274-278.	7.2	56
120	Determination of optical birefringence by using off-axis transmission ellipsometry. Applied Optics, 2005, 44, 3153.	2.1	14
121	A laser-deposition approach to compositional-spread discovery of materials on conventional sample sizes. Measurement Science and Technology, 2005, 16, 21-31.	1.4	20
122	Pulsed electron deposition of fluorine-based precursors for YBa2Cu3O7â^'x-coated conductors. Superconductor Science and Technology, 2005, 18, 1168-1175.	1.8	19
123	Thermal stability of epitaxial SrRuO3 films as a function of oxygen pressure. Applied Physics Letters, 2004, 84, 4107-4109.	1.5	71
124	High-throughput growth temperature optimization of ferroelectric SrxBa1â^'xNb2O6 epitaxial thin films using a temperature gradient method. Applied Physics Letters, 2004, 84, 1350-1352.	1.5	31
125	Surface/Interface-Related Conductivity in Nanometer Thick YSZ Films. Electrochemical and Solid-State Letters, 2004, 7, A459.	2.2	76
126	Continuous composition-spread thin films of transition metal oxides by pulsed-laser deposition. Applied Surface Science, 2004, 223, 35-38.	3.1	49

#	Article	IF	CITATIONS
127	An improved continuous compositional-spread technique based on pulsed-laser deposition and applicable to large substrate areas. Review of Scientific Instruments, 2003, 74, 4058-4062.	0.6	49
128	Influence of MgO substrate miscut on domain structure of pulsed laser deposited SrxBa1â^'xNb2O6 as characterized by x-ray diffraction and spectroscopic ellipsometry. Applied Physics Letters, 2003, 82, 2990-2992.	1.5	20
129	Growth of oxide seed layers on ni and other technologically interesting metal substrates: issues related to formation and control of sulfur superstructures for texture optimization. IEEE Transactions on Applied Superconductivity, 2003, 13, 2646-2650.	1.1	15
130	Time-resolved study of SrTiO3 homoepitaxial pulsed-laser deposition using surface x-ray diffraction. Applied Physics Letters, 2002, 80, 3379-3381.	1.5	59
131	Characterization of linear diattenuator and retarders using a two-modulator generalized ellipsometer (2-MGE). , 2002, , .		2
132	Spectroscopic Ellipsometry Studies of Nanocrystalline Silicon in Thin-Film Silicon Dioxide. Materials Research Society Symposia Proceedings, 2002, 737, 319.	0.1	0
133	Transmission two-modulator generalized ellipsometry measurements. Applied Optics, 2002, 41, 6555.	2.1	29
134	Superconducting magnesium diboride films with Tcâ‰^24 K grown by pulsed laser deposition with in situ anneal. Physica C: Superconductivity and Its Applications, 2001, 353, 157-161.	0.6	69
135	Blue photoluminescence in ZnGa[sub 2]O[sub 4] thin-film phosphors. Journal of Applied Physics, 2001, 89, 1653.	1.1	63
136	Epitaxial Growth and Luminescent Properties of Mn2+-Activated ZnGa2O4 Films. , 2000, 4, 293-297.		7
137	Pulsed KrF laser deposited GaN/TiN/Si(111) heterostructures by sequential TiN and liquid Ga laser ablation. Applied Physics A: Materials Science and Processing, 1999, 69, S441-S445.	1.1	6
138	Silicon and zinc telluride nanoparticles synthesized by low energy density pulsed laser ablation into ambient gases. Journal of Materials Research, 1999, 14, 359-370.	1.2	48
139	ZnGa2O4 Thin-Film Phosphors Grown by Pulsed Laser Ablation. Materials Research Society Symposia Proceedings, 1999, 560, 59.	0.1	0
140	Heteroepitaxial growth of n-type CdSe on GaAs(001) by pulsed laser deposition: studies of film–substrate interdiffusion and indium diffusion. Journal of Crystal Growth, 1998, 193, 516-527.	0.7	9
141	Silicon and zinc telluride nanoparticles synthesized by pulsed laser ablation: size distributions and nanoscale structure. Applied Surface Science, 1998, 127-129, 355-361.	3.1	51
142	Growth of p-type ZnTe and n-type CdSe films on GaAs(001) by pulsed laser ablation. Applied Surface Science, 1998, 127-129, 418-424.	3.1	32
143	Study of Substrate Diffusion in Epitaxial N-Type CdSe Films Grown on GaAs (001) by Pulsed Laser Ablation. Materials Research Society Symposia Proceedings, 1998, 526, 27.	0.1	3
144	Amorphous Diamond Films Deposited by Pulsed-Laser Ablation: the Optimum Carbon-Ion Kinetic Energy and Effects of Laser Wavelength. Materials Research Society Symposia Proceedings, 1998, 526, 325.	0.1	18

#	Article	IF	CITATIONS
145	Synthesis of Novel Thin-Film Materials by Pulsed Laser Deposition. Science, 1996, 273, 898-903.	6.0	547
146	Growth of Highly Doped P-Type Znte Films by Pulsed Laser ablation in Molecular Nitrogen. Materials Research Society Symposia Proceedings, 1995, 388, 85.	0.1	0
147	Pulsed Laser Ablation Growth and Doping of Epitaxial Compound Semiconductor Films. Materials Research Society Symposia Proceedings, 1995, 397, 107.	0.1	4
148	Growth of highly doped pâ€ŧype ZnTe films by pulsed laser ablation in molecular nitrogen. Applied Physics Letters, 1995, 67, 2545-2547.	1.5	38
149	Dislocations in latticeâ€mismatched wideâ€gap IIâ€VI/GaAs heterostructures as laser light scatterers: Experiment and theory. Journal of Applied Physics, 1995, 78, 1203-1209.	1.1	15
150	p-type ZnSe : N grown by molecular beam epitaxy: evidence of non-radiative recombination centers in moderately to heavily doped material. Journal of Crystal Growth, 1994, 138, 352-356.	0.7	3
151	GaAs substrate cleaning for epitaxy using a remotely generated atomic hydrogen beam. Journal of Applied Physics, 1993, 73, 4610-4613.	1.1	42
152	In situ, realâ€ŧime diffuse optical reflectivity measurements during GaAs cleaning and subsequent ZnSe/GaAs heteroepitaxy. Journal of Vacuum Science and Technology A: Vacuum, Surfaces and Films, 1993, 11, 1792-1795.	0.9	13
153	Design and implementation of a magnetic drive retrofit to the Vacuum Generator's venetian style viewport shutter assembly. Journal of Vacuum Science and Technology A: Vacuum, Surfaces and Films, 1993, 11, 464-465.	0.9	2
154	Insiturealâ€ŧime determination of the freeâ€carrier density in doped ZnSe films during molecular beam epitaxial growth. Applied Physics Letters, 1992, 60, 2723-2725.	1.5	10
155	Strain-free, ultra-high purity ZnSe layers grown by molecular beam epitaxy. Journal of Materials Research, 1990, 5, 475-477.	1.2	20
156	pâ€ŧype ZnSe by nitrogen atom beam doping during molecular beam epitaxial growth. Applied Physics Letters, 1990, 57, 2127-2129.	1.5	622
157	Simulation of the Impact of Point Defects and Edge Dislocations on Xâ€Ray Diffraction in Hexagonal (Ni,Co) _{1+2 <i>x</i>} Ti _{1â° <i>x</i>} O ₃ Thin Films. Physica Status Solidi (B): Basic Research, 0, , 2100583.	0.7	0